Imad *et al.*
Journal of Engineering and Applied Science (2023) 70:141
https://doi.org/10.1186/s44147-023-00318-1

Journal of Engineering and Applied Science

RESEARCH Open Access

Modelling of asymmetric channel plasmonic polariton waveguides

Saja Imad[1], Riyadh Mansoor[2*], Rasha Ali[3] and Fras Hussain[3,4]

*Correspondence:
riyadhdmu@mu.edu.iq

[1] General Directorate of Muthanna Education, the Ministry of Education, Samawa, Iraq
[2] Electronics and Communication Engineering, Al-Muthanna University, Samwa, Iraq
[3] Physics Department, College of Science, Al-Muthanna University, Samawa, Iraq
[4] Technical Engineering College, Al-Ayen Iraqi University, Nasiriyah, Thi-Qar, Iraq

Abstract

Channel plasmonic polariton (CPP) waveguides are a promising technology for integrated photonics. They offer several advantages over other plasmonic waveguides and are well-suited for various applications. In this research, a new design of asymmetric double-trenched CPP waveguide is suggested and examined. This design consists of two silicon trenches etched into a silicon dioxide substrate layer; with a gold layer sandwiched in between. The trenches are asymmetric, with one trench being wider than the other. This asymmetry creates a spatially varying surface plasmon polariton (SPP) field, which can guide light along the waveguide. The polarization characteristics of this proposed design are analyzed over a specific wavelength range (0.7 — 1.7 μm) to evaluate the mode confinement of the light within the structure. The design performance was optimized by changing the gold layer thickness and the dimensions of the lower trench. Different scenarios are examined to observe TE and TM-polarized modes' behavior within the groove. A 1867.119 dB/μm suppression level at 0.92 μm wavelength is achieved which offers a small-size component for compact photonic logic gates, enabling the development of next-generation photonic devices.

Keywords: CPP, Finite element method, NOR gating, Plasmonic waveguide, Photonics

Introduction

Surface plasmon polariton (SPP)-based all-optical signal processing devices are currently receiving a lot of attention in optical communication systems [1, 2]. Plasmonic is a branch of science that studies the behavior and manipulation of plasmons, which are collective oscillations of electrons in metal when excited by light. It focuses on the interaction between light and metal surfaces or nanostructures, enabling the confinement and manipulation of light at nanoscale dimensions [3–5]. Plasmonics has applications in various fields, such as photonics [6], nanophotonics [7], optoelectronics [8], and sensing [9, 10]. To enable light to concentrate beyond its diffraction limit, these EM waves' distribution can be modified using a variety of techniques. These EM fields degrade exponentially into the boundaries [11, 12]. Future designs of nanophotonics logic gates and devices will benefit greatly from SPP waveguides' extraordinary capacity to focus and control light in regions with profound wavelengths. SPP

waveguides are used by specific utilitarian plasmonic segments and extras to carry out their desired function [13] such as plasmonic sensors [14, 15] and plasmonic modulators [16, 17]. SPP-based all-optical plasmonic devices provide good logical gate design candidates for a variety of factors. First, they are significantly smaller than contemporary electronic logic gates, which are centimeter-sized, and have dimensions in the order of nanometers. A second benefit is that they execute logic operations at the speed of light Furthermore, Kerr nonlinear plasmonic resonators outperform linear plasmonic waveguides by changing the intensity of the pumps, not the metal's refractive index. Finally, the resonance in light waves that submit to Kerr nonlinear waveguides makes it simple to determine the transmission rate [18–20]. A new asymmetric CCP waveguide design is proposed in this research. It suggests the use of a two-trench asymmetric waveguide for NOR gating. To evaluate the performance of the suggested designs, the real effective index (n_{eff}) and propagation loss (dB/μm) are studied in the presence of gold (Au) as metal between silicon and silicon dioxide substrate. The numerical calculations are performed based on the Finite Element Method (FEM) [21, 22] using Multiphysics simulation software. The suggested CPP-based waveguide is examined with different design dimensions for the trench to evaluate filter's the performance through the calculation of the cutoff frequency. Maximizing the cutoff suppression level at the required wavelength allows for a NOR gate behavior of the suggested design which allows for small-size logic components for high-dense photonic integrated circuits.

The remaining of this paper is structured as follows: the basic consideration of the CCPs are presented in the "Basic considerations of the CPP Model" and the "Simulation method" sections. In the "Results and discussion" section, the simulation results are presented and discussed. The conclusion is in the "Conclusions" section.

Basic considerations of the CPP Model

Figure 1 shows the 3D diagram of the CPP-based waveguide design. Here, it can easily be noted how silicon (Si) forms double trenches on silicon dioxide (SiO_2) substrate. This design (Fig. 1a and b) is said to be asymmetric since the dimensions of the upper and lower trenches are different compared to those in Fig. 1c. The symmetry of the design requires the total depth of the silicon trench (d) to be divided equally between the upper and lower ones, i.e. $d_1 = d_2 = d_3$. Also, the upper trench is wider compared to the lower one ($w_1 > w_2$). Moreover, a thin gold layer has been added between the Si and SiO_2 materials in order to increase the mode confinement depending on the plasmonic effect. This layer has a thickness (d_4) which has been varied from 50 to 150 nm with 50-nm step. Additionally, the blue arrow in Fig. 1b and c represents the incident light on the trench.

For the proposed asymmetric design (Fig. 1a), there is another dimension that needs to be considered for the lower trench which is d_3. The total groove depth is kept to be $d = d_1 + d_2$. However, the shape of the upper and lower trenches is irregular, especially for the lower one where the left side depth is $d_3 \neq d_2$. For our design consideration, d_3 is changed from 0.2 to 0.4 μm to estimate the effect of the design asymmetry on mode confinement.

CPP-based waveguides support the transmission of two dominant modes TM (X-polarized) and TE mode (Y-polarized). The main difference between TE and TM

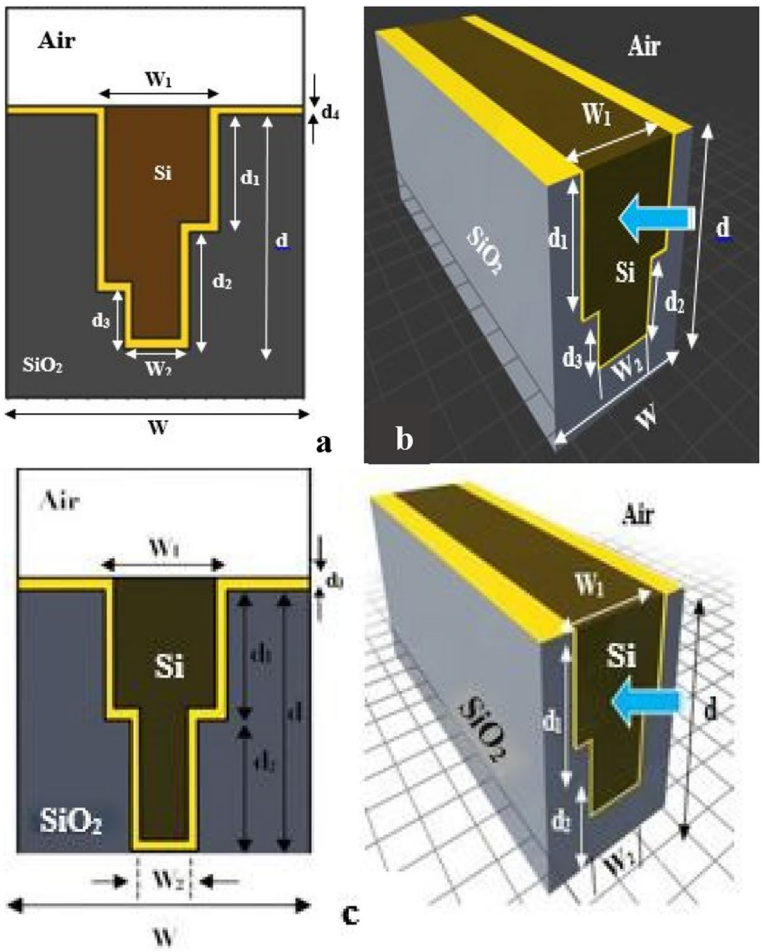

Fig. 1 **a** and **b** Asymmetric double-trenched CPP waveguide. **c** Symmetric model

modes in channel plasmon polariton waveguides is the direction of the electric field. In TE modes, the electric field is perpendicular to the direction of propagation, while in TM modes, the electric field is parallel to the direction of propagation. This difference in polarization leads to different propagation characteristics for TE and TM modes. TE modes have a higher cutoff frequency than TM modes, meaning that they can only propagate at higher frequencies. TE modes also have a lower group velocity than TM modes, meaning that they travel slower. In addition to the difference in propagation characteristics, TE and TM modes also have different confinement properties. TE modes are more confined to the core of the waveguide than TM modes. This is because the electric field in TE modes is concentrated in the core, while the electric field in TM modes is also present in the cladding. The choice of TE or TM mode for a channel plasmon polariton waveguide depends on the specific application. For applications where a high cutoff frequency is required, TE mode is typically the better choice. For applications where a high group velocity is required, TM mode is typically the better choice. And for applications where high confinement is required, TE mode is typically the better choice.

A metal substrate is inserted between the Si and SiO_2 substrate as shown in Fig. 1a. This layer will ensure the generation of the plasmonic effect in the boundaries and

couple with one of the fundamental modes, leaving the other mode to pass the waveguide without coupling (low loss). The coupling mechanism in the proposed design is highly affected by the structure dimensions as will be seen in the following sections.

Simulation method

COMSOL Multiphysics solver which relays on the FEM method is used to simulate the proposed design and examine the effect of structure dimensions on the overall performance. A 6232 triangle parts with 12,139 degrees of freedom are used to analyze the cross-section of the proposed CPP structure. Also, the X and Y sides' computational ranges are 1.5 and 2 μm. Simulation results are focusing on the polarization properties of the asymmetric model taking into account the effect of the lower trench dimension on the modes' confinement. Different scenarios are tested to study the overall performance of the proposed design with the use of gold as a metal layer between Si and SiO_2.

Initially, the design dimensions are chosen as follows: $d_1 = 0.6$ μm, $w_1 = 0.523$ μm, and $w_2 = 0.24$ μm, while the total depth of the groove (d) is 1.2 μm. The gold thickness is 50 nm. The design metrics consist of the d_3 and gold thickness. However, the suggested design's performance is evaluated concerning n_{eff} and losses over the selected wavelength range. For each selected set of dimensions, n_{eff} and loss for the two fundamental modes are plotted and the cutoff wavelength for each mode is measured. The results reveal the mode confinement depends on the shape change of the lower trench as well as the metal material thickness. The proposed design can be optimized to be used based on the required application as it offers a high degree of control for the TE and TM modes.

The choice of TE or TM mode for a channel plasmon polariton waveguide depends on the specific application like the cutoff frequency. If it is required to guide light at a high frequency, then TE mode is the better choice. This is because TE modes have a higher cutoff frequency than TM modes. In general, TE mode is a better choice for applications where high cutoff frequency and high confinement are important. TM mode is a better choice for applications where high group velocity is important [23, 24].

Results and discussion

As mentioned in the previous section, the following calculations will depend on the changing of gold material thickness (d_4) as well as the lower trench left side depth (d_3). A specific range for d_3 and d_4 is selected to control the iteration's times. Three degrees of asymmetry for the lower trench are tested based on the value of d_3; namely, 0.2 (high asymmetry), 0.3 (medium asymmetry), and 0.4 μm (low asymmetry) are selected. The normal case of no asymmetry (symmetrical DCP) occurred for $d_3 = d_2 = 0.6\ \mu$m (Fig. 1c). The behavior of the symmetric design is depicted in Fig. 2. In terms of loss, there are two rapid jumps in the Y-polarized mode at wavelength 0.925 μm and 1.35 μm, respectively. In this case, the TE (Y-polarized) mode has a high loss of 21.46 dB/μm at the operating wavelength 0.925 μm On the other hand, the weak confined TM (X-polarized) mode has a low loss of 3.66 dB/μm at the same wavelength. Moreover, the highest peak loss for Y-polarized mode is equal to 16.95 dB/μm at wavelength 1.35 μm, while X-polarized has a low loss of 8.48 dB/μm at the same wavelength.

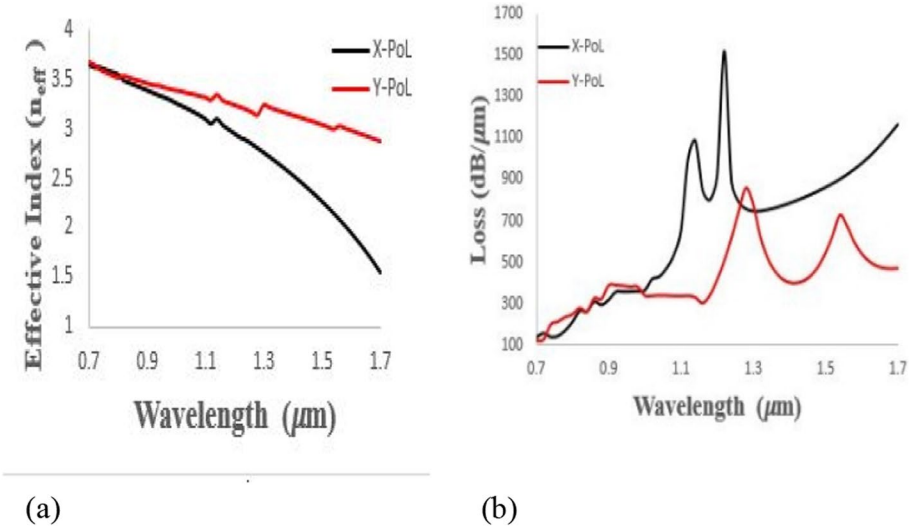

Fig. 2 Loss (dB/μm) of the *Y*-polarized (in red lines), and *X*-polarized (in blue lines) as a function of wavelength for 2-trench CPPs with Au thickness 50 nm, $w_1 = 0.532$ μm, $w_2 = 0.24$ μm, d_1 and $d_2 = 0.6$ μm

High asymmetry ($d_3 = 0.2$ μm)

For $d_4 = 50$ nm, TE and TM modes behavior within the proposed design can be estimated through the calculation of the real part of the effective refractive index as well as the loss along the selected wavelength range. The real part of the (n_{eff}) can be used to determine the dispersion characteristics of the waveguide, while the cutoff wavelength of the waveguide can be achieved from the loss response.

Figure 2 shows that both the TE and TM modes exhibit a decrease in the real part of the effective refractive index for longer wavelengths. Also, n_{eff} of the TE and TM guided modes has almost the same value for the shorter range of wavelengths (from 0.7 μm to 0.92 μm). The most important indication in the proposed design response can be estimated from the loss response (Fig. 2b) where two rapid changes in the *X*-polarized mode at two wavelengths, namely 1.14 μm and 1.22 μm, are shown. These are an indication of the plasmonic resonance occurrence and the high-mode confinement through the groove (1088.96 dB/μm at the operating wavelength 1.14 μm). However, the TE (*Y*-polarized) mode shows lower confinement at the same wavelength (327.402 dB/μm). On the other hand, a comparison of the loss for the two modes at 1.22 μm wavelength shows that the *X*-polarized mode is prone to 1521.39 dB/μm loss compared to 505.848 dB/μm for the *Y*-polarized mode. Moreover, there are two rapid jumps in the losses of the TE modes which are equal to 860.75 dB/μm, and 728.895 dB/μm at operating wavelength 1.28 μm, and 1.54 μm, respectively.

For lower frequencies (longer wavelengths) unvarying TM mode transmission through the groove is achieved.

For $d_4 = 100$ nm: In this design scenario, the suppression level peaks of the *X*-polarized mode keep occurring at the same wavelength with different levels of the previous case. Here, losses of 1341.16 and 986.87 dB/ μm for the TM mode at wavelength 1.14, 1.22 μm respectively can be noted compared to 294.844, and 525.457 dB/ μm for the *Y*-polarized mode at the same frequency. Moreover, the TE mode faces a higher suppression level of 1066.727 and 638.138 dB/ μm at shorter wavelengths, 1.26 and 1.52 um respectively, as shown in Fig. 3.

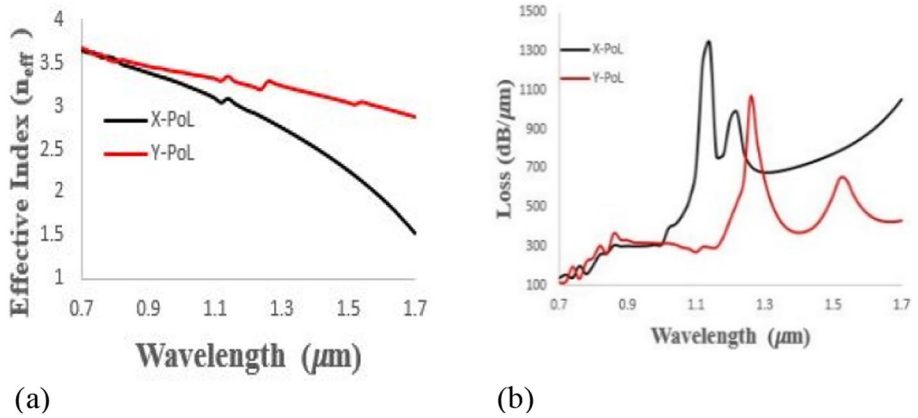

Fig. 3 Polarization response (effective refractive index (**a**) and loss (**b**)) for scenario 2 asymmetric CPPs with $w_1 = 0.532$ µm, $w_2 = 0.24$ µm, $d_1 = d_2 = 0.6$ µm, and $d_3 = 0.2$ µm and the Au thickness is 100 nm

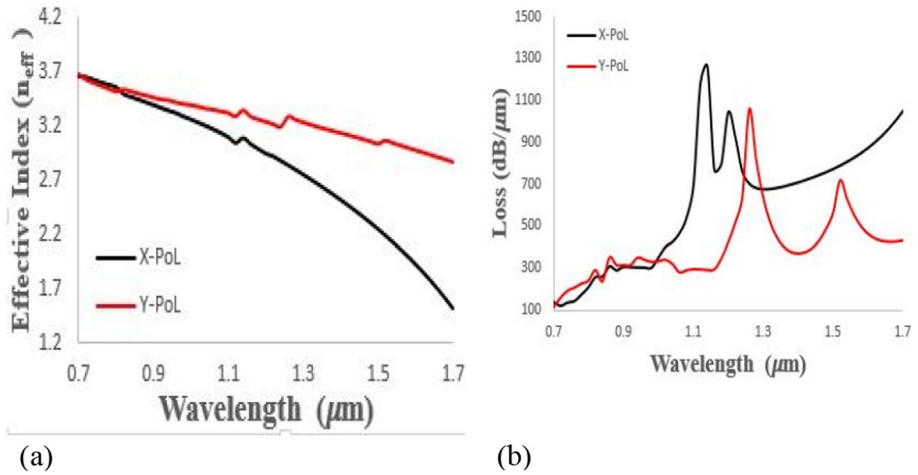

Fig. 4 Polarization response (effective refractive index (**a**) and loss (**b**)) for Scenario 3 asymmetric CPPs with $w_1 = 0.532$ µm, $w_2 = 0.24$ µm, $d_1 = d_2 = 0.6$ µm, and $d_3 = 0.2$ µm and the Au thickness is 150 nm

For $d_4 = 150$ nm: The two modes are very close to each other in terms of n_{eff} at the wavelength range of 0.7 to 0.94 µm, then a big change is occurring for the low frequencies as shown in Fig. 4a. Figure 4b shows the loss values for *X*-polarized modes which are 1265.232, and 1046.795 dB/µm at 1.14, and 1.2 µm wavelengths, respectively, while for the same wavelength, it is 291.206, 424.139 dB/µm for the *Y*-polarized mode. That means the TE mode can travel free of loss in this wavelength range. However, high loss peaks of 1056 and 614 dB/µm occur at longer wavelengths.

Finally, it can be seen that for $d_3 = 0.2$ µm and for three different values of the gold material thickness, the designed waveguide shows a high suppression level for the *X*-polarized mode in the high-frequency range (1.12 to 1.28 µm wavelength), while for low frequency this mode is passing the trench unaffected.

Medium asymmetry (d3 = 0.3 μm)

A similar procedure to that applied in the "High asymmetry (d3 = 0.2 μm)" section is repeated here with the increase in the area of the lower trench by increasing the left side

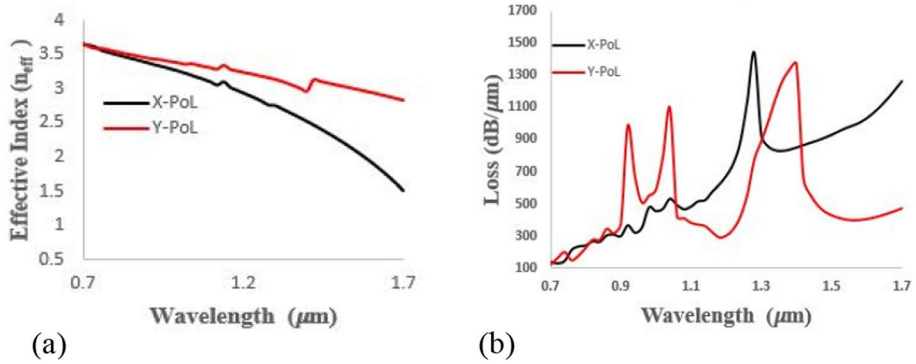

Fig. 5 Polarization response (effective refractive index (**a**) and loss (**b**)) for Scenario 4 asymmetric CPPs with $w_1 = 0.532$ µm, $w_2 = 0.24$ µm, $d_1 = d_2 = 0.6$ µm, and $d_3 = 0.3$ µm and the Au thickness is 50 nm

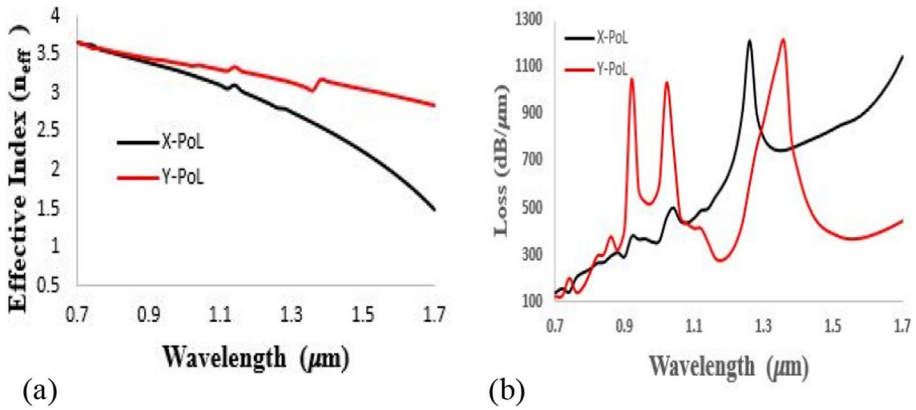

Fig. 6 Polarization response (effective refractive index (**a**) and loss (**b**)) for Scenario 5 asymmetric CPPs with $w_1 = 0.532$ µm, $w_2 = 0.24$ µm, $d_1 = d_2 = 0.6$ µm, and $d_3 = 0.3$ µm and the Au thickness is 100 nm

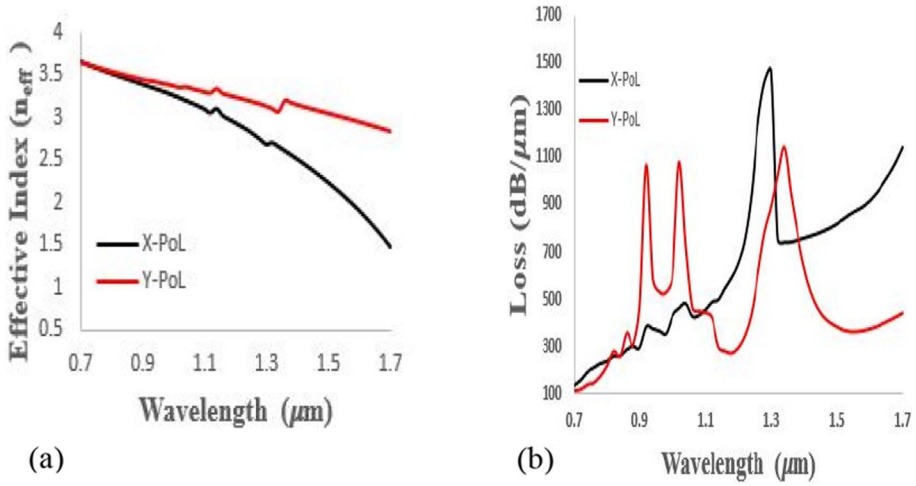

Fig. 7 Polarization response (effective refractive index (**a**) and loss (**b**)) for Scenario 6 asymmetric CPPs with $w_1 = 0.532$ µm, $w_2 = 0.24$ µm, $d_1 = d_2 = 0.6$ µm, and $d_3 = 0.3$ µm and the Au thickness is 150 nm

depth d_3 to 0.3 μm. Again, three different values of the gold thickness are tested with the new geometry of the asymmetric trench, and the model response of each scenario is obtained. Figures 5, 6, and 7 are obtained for $d_4 = 50$, 100, and 150 nm, respectively.

The performance of the model with $d_4 = 50$ nm is presented in Fig. 5. It is obvious from Fig. 5a that the two fundamental modes are closely situated from 0.7 to 0.84 μm wavelength. Then, there are sudden changes appear for the TE mode at 0.92, 1.04, and 1.4 μm, with one peak for the TM mode at 1.28 μm. Furthermore, the loss behavior of both modes as illustrated in Fig. 5b shows that the TM mode propagates inside the waveguide unaffected in its path at the boundaries at the wavelengths 0.7 to 1.24 μm. This reveals that it is restricted within the groove due to the resonant plasmonic frequency. Subsequently, it exhibits the peak suppression level reaching up to 1442.017 dB/μm at 1.28 μm wavelength, while the *Y*-polarized mode loss is 770.70 dB/μm at the same wavelength. The TE mode peak losses are 986.38, 1095.49, and 1372.6 dB/μm at 0.92, 1.04, and 1.4 μm respectively.

From Fig. 6, where d_4 is increased to 100 nm, it can be noted that for long wavelengths, the n_{eff} is marginally decreasing. Also, in the range of 0.7 to 0.86 μm, the two fundamental modes show a similar response in Fig. 6a. That decrease in the n_{eff} is coordinated with a high suppression level as indicated in Fig. 6b. The loss behavior at 100 nm is the same as the loss behavior at 50 nm, but here, it is evident that there is an increase in suppression level compared to the previous one getting to 1048.73, 1030.13, and 1204.4 dB/μm for TE mode at 0.92, 1.02, and 1.36 μm, respectively. Also, it reveals a good filter performance at certain wavelengths 0.92 and 1.02 μm due to the passage of one mode and the cancellation of the other mode at the same wavelength. Additionally, the peak at this wavelength has a narrower bandwidth compared to the others, such as the peak at wavelength 1.36 μm. Moreover, the loss behavior for the *X*-polarization is the same when the plasmonic material thickness was 50 nm.

Lastly, for $d_4 = 150$ nm, Fig. 7a presents the wavelength dependence of the real part of n_{eff} and loss for the two dominant modes which are almost touching each other from 0.7 to 0.88 μm. Afterwards, the two modes diverge as the wavelengths increase, with a noticeable emergence of some peaks for the two modes.

From Fig. 7b, it is evident that there is an increase in suppression level compared to the previous one to 1066.764, 1077.48, and 1140.822 dB/μm for the TE mode at wavelength 0.92, 1.02, and 1.34 μm, respectively. Also, it obtains a good filter at certain wavelengths (0.92 and 1.02 μm) because of the transmission of one mode and the nullification of the other mode at the identical wavelength, there is an additional observation of a narrower bandwidth for the peak at this wavelength compared to the rest, such as the peak at 1.34 μm. Moreover, the loss behavior for the *X*-polarization shows a 1468.03 dB/μm loss at 1.3 μm wavelength.

Low asymmetry (d3 = 0.4 μm)

Figure 8a shows the real part of the n_{eff} for two modes and their relation with wavelength for $d_4 = 50$ nm; again the two modes are proximate to each other over the 0.7 to 0.86 μm range, and for longer wavelengths, they are getting further away from each other with some abrupt changes appear at 0.94, 1.06, and 1.36 μm for TE mode and at 1.36 μm for

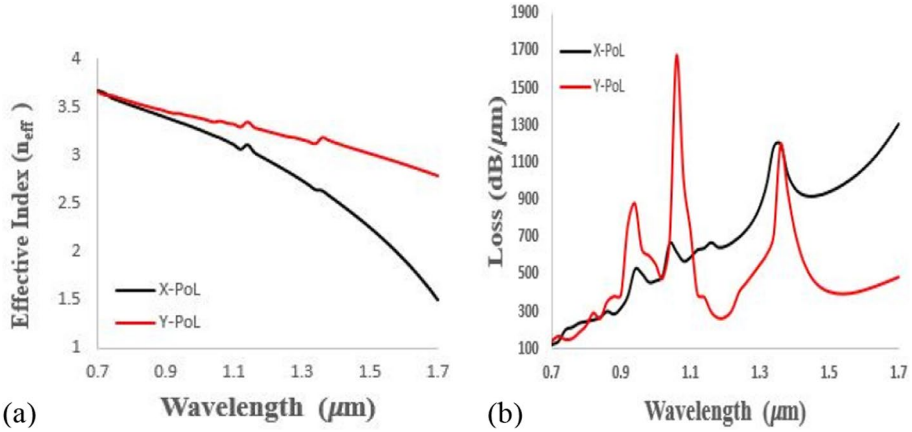

Fig. 8 Polarization response (effective refractive index (**a**) and loss (**b**)) for Scenario 7 asymmetric CPPs with $w_1 = 0.532$ µm, $w_2 = 0.24$ µm, d1 = d2 = 0.6µm. and d3 = 0.4 µm and the Au thickness is 50 nm

X-polarized modes; it is due to the field is a good confined inside the groove. This reduction in the n_{eff} is alongside an increase in loss behavior as presented in Fig. 8b; for *Y*-polarized modes (TE), there are three peaks of loss at different wavelengths: 0.92, 1.06, and 1.36 µm. The highest one was at a wavelength of 1.06 µm, where the loss value reached 1674.321 dB/ µm; it achieved a good filter at this point due to the narrow peak bandwidth, where one mode passed and the other was cancelled at the same wavelength. Additionally, there was a clear loss for the TM mode, reaching 1196.12 dB/ µm and 1195.75 dB/ µm for the TE mode at 1.36 µm.

The gold thickness of $d_4 = 100$ nm is also studied, as shown in Fig. 9. The wavelength dependency of n_{eff} and losses for the two dominant modes are nearby at the wavelengths range from 0.7 to 0.86 µm. This is caused by plasmonic resonance frequency. Then the two modes are speared away from each other by increasing wavelength. Moreover, sudden change in the n_{eff} occurs at 0.92, 1.06, and 1.36 µm for the TE mode and 1.34 µm for the TM mode as depicted in Fig. 9a. However, Fig. 9b shows the suppression level curve of the *X*-polarization that does not suffer from any change throughout its propagation inside the groove over the 0.7 µm to 1.7 µm wavelength range, except for a small peak

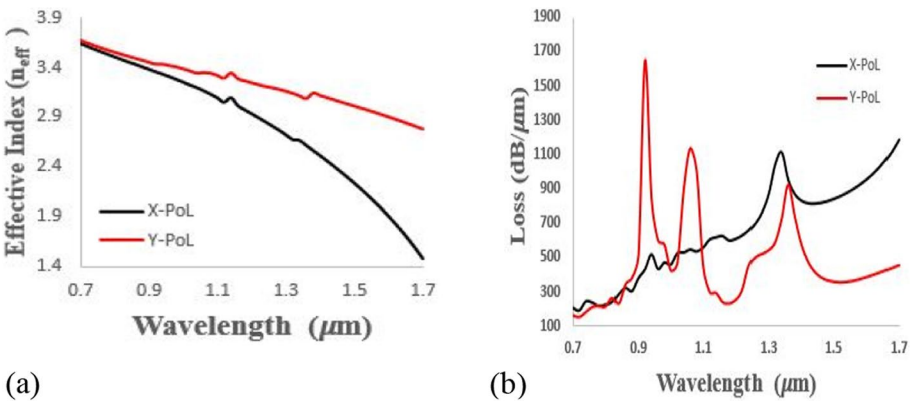

Fig. 9 Polarization response (effective refractive index (**a**) and loss (**b**)) for Scenario 8 asymmetric CPPs with $w_1 = 0.532$ µm, $w_2 = 0.24$ µm, $d_1 = d_2 = 0.6$ µm, and $d_3 = 0.4$ µm and the Au thickness is 100 nm

reaching 1112.52 dB/μm at 1.34 μm. TM mode remains unchanged as the wavelengths continue to increase because, in this case, the mode tries to stay within the trench and adheres to the plasmonic material.

On the other hand, for the *Y*-polarization, the peak value is 1644.785 dB/μm at a wavelength of 0.92 μm making this structure act as an excellent filter for this mode due to the narrow peak bandwidth. Another two loss values at a wavelength of 1.06 and 1.36 μm are obtained, and as the wavelengths increase above 1.38 μm, it is noticed that there is no change in the two modes as they pass through the trench.

Figure 10a illustrates the two modes have almost the same response along the wavelength span from 0.7 to 0.86 μm when the Au thickness is equal to 150 nm, then they depart from each other for longer wavelengths. Also, unexpected spikes emerge due to the effect of plasmonic resonant at wavelengths 0.92, 1.06, and 1.36 μm, concerning TE mode and at 1.34 μm at the TM mode.

Additionally, the TE mode has a higher loss compared to the *X*-polarized mode as evident in Fig. 10b because of the high confinement inside the wide trench. An excellent band rejection filter performance is expected because of the narrow bandwidth with a suppression level equal to 1867.119 dB/μm at wavelength 0.92 μm. Other values of loss 1227.269 and 956.709 dB/μm at 1.06 and 1.36 μm respectively are obtained. Additionally, TM modes have a weak suppression level equal to 1126.85 dB/ μm at 1.34 μm. Then for longer wavelengths (above 1.42 μm), an increase in the loss behavior is observed.

Conclusions

Asymmetric double trench CPP waveguides have several advantages over other types of plasmonic waveguides. They are more robust to scattering, which makes them less susceptible to losses. They are also more efficient at coupling light into and out of the waveguide. As a result, CPP waveguides are well-suited for applications in integrated photonics, such as sensors and optical interconnects. The properties of such waveguides can be controlled by adjusting the geometry of the trenches. The trench width, and depth, as well as the thickness of the dielectric layer, all affect the propagation characteristics of the SPPs. By carefully optimizing these parameters, it is possible to design asymmetric CPP waveguides with a wide range of properties, such as different bandwidths,

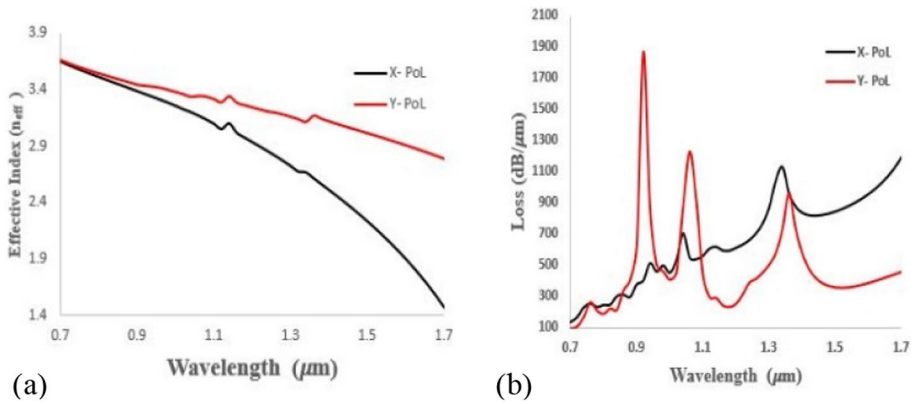

Fig. 10 Polarization response (effective refractive index (**a**) and loss (**b**)) for Scenario 9 asymmetric CPPs with $w_1 = 0.532$ μm, $w_2 = 0.24$ μm, $d_1 = d_2 = 0.6$ μm, and $d_3 = 0.4$ μm and the Au thickness is 150 nm

losses, and coupling efficiencies. In this work, a silicon-on-insulator-based CPP waveguide design is suggested and thoroughly investigated. A gold layer is inserted between the silicon groove and the silicon dioxide substrate. The design performance was optimized in terms of the gold layer thickness and the dimensions of the lower trench. Different scenarios were examined to observe the dispersion characteristics of the proposed model. The two dominant modes' behavior within the groove is studied over a specific wavelength range. It was noticed that the proposed model exhibits at certain wavelengths (for a certain polarized mode), which can play an important role in the development of next-generation photonic devices.

Abbreviations

CCP	Channel plasmon polariton
EM	Electromagnetic
SPP	Surface plasmon polariton
FEM	Finite element method
DT	Doubl trenched
TE	Transverse electric
TM	Transverse magnetic

Acknowledgements
To Al Muthanna University for continuous support.

Authors' contributions
First author: simulation. Second author: writing, editing, and discussion. Third and fourth authors: calculations.

Funding
No funding.

Availability of data and materials
Not applicable.

Declarations

Competing interests
The authors declare that they have no competing interests.

Received: 24 August 2023 Accepted: 9 November 2023
Published online: 20 November 2023

References

1. Falah FH, Mansour TS (2019) Design and simulation of all-optical plasmonic logic gates based on nano-ring insulator-metal-insulator waveguides. Int J Adv Sci Technol 29(3):405–425
2. Mansoor R, AL-Khursan AH (2018) Numerical modelling of surface plasmonic polaritons. Results Phys 9:1297–1300
3. Feng Y, Liu Y, Shi Y, Teng J (2018) Tunable plasmonic filter based on graphene-layered waveguide. Modern Phys Lett B 32(08):1850110
4. Saeidi P, Jakoby B, Pühringer G, Tortschanoff A, Stocker G, Spettel J, Dubois F, Grille T, Jannesari R (2022) Design, analysis, and optimization of a plasmonic slot waveguide for mid-infrared gas sensing. Nanomaterials. 12:1732
5. Ou W, Zhou B, Shen J, Zhao Ch, Li YY, Lu J (2021) Plasmonic metal nanostructures: concepts, challenges and opportunities in photo-mediated chemical transformations. Science. 24(2):101982
6. Elbanna A, Jiang H, Fu Q, Zhu JF, Liu Y, Zhao M, Liu D, Lai S, Chu XW, Pan J, Shen ZX, Wu L, Liu Z, Qiu CW, Teng J (2023) 2D material infrared photonics and plasmonics. ACS Nano 17(5):4134–4179
7. Gomes AS, Menezes LD, de Oliveira HP (2023) Nanophotonics in modern plasmonics and nanolasers. In: Modern Luminescence from Fundamental Concepts to Materials and Applications 2023 Jan 1 (pp. 275-312). Woodhead Publishing
8. Salim ET, Shafeeq SR, AbdulRazzaq MJ, Fakhri MA, Gopinath SCB (2023) Photo-activation of Ag chemicals for enhanced Nb2O5 optoelectronic device employing plasmonic effects. Surfaces and Interfaces 36:102618
9. Kirk A (2023) Plasmonic nanostructures for sensing. Encyclopedia of Materials: Electronics. p. 176–192
10. Zhang K, Luo M, Rao H, Liu H, Li J, Chen J, Liu X, Xue Z (2023) Integrating plasmonic and nanozyme responses of gold nanoparticles for enhancing photothermometric sensing. Sensors and Actuators B: Chemical 134067
11. Mansoor R, Hussain FFK, Ali R (2019) Dispersion characteristics of asymmetric multistep titanium nitride channel plasmon waveguide. Proceedings of the International Conference on Information and Communication Technology
12. Smith CLC, Stenger N, Kristensen A, Mortensen NA, Bozhevolnyi SI (2015) Gap and channelled plasmons in tapered grooves: a review. Nanoscale 7:9355

13. Wei H, Pana D, Xu H (2015) Design and simulation of all-optical plasmonic logic gates based on nano-ring insulator-metal-insulator waveguides routing of surface plasmons in silver nanowire networks controlled by polarization and coating. Nanoscale 7:19053–19059
14. Danaie M, Kiani B (2018) Design of a label-free photonic crystal refractive index sensor for biomedical applications. Photonics Nanostruct Fundam Appl 31:89
15. Islam MS, Sultana J, Rifat AA, Ahmed R, Dinovitser A, Ng BWH, Heidepriem HE, Abbott D (2018) Dual-polarized highly sensitive plasmonic sensor in the visible to near-IR spectrum. Opt Express. 26:30347–30361
16. Chauhan D, Sbeah Z, Dwivedi RP, Nunzi JM, Thakur MS (2022) An investigation and analysis of plasmonic modulators: a review. J Opt Commun
17. Liu W, Yang K, Zhang W, Hao M, Wen K, Hu X, Qin Y (2023) Tunable plasmonic modulator with high-modulation-depth through electrical control. Optics Commun 528:129009
18. Mei X, Huang XG, Jin T (2011) A sub-wavelength electro-optic switch based on plasmonic T-shaped waveguide. Plasmonics 6(4):613–618
19. Peng X, Li H, Wu C, Cao G, Liu Z (2013) Research on transmission characteristics of aperture-coupled square-ring resonator based filter. Optics Commun 294:368–371
20. Ghadi A, Darzi B (2023) All-optical nano logical gates AND, NOR, OR, and NOT based on plasmonic waveguides with Kerr nonlinear cavity. Optics Laser Technol 157:108651
21. Volakis JL, Chatterjee A, Kempel LC (1998) Finite element method for electromagnetics. Universities Press; 1998
22. Bhavikatti SS (2005) Finite element analysis. New Age International
23. Hussain FFK et al (2022) Analysis of efficient polarization filter based on double trenched channel plasmon polariton waveguides. Solid State Commun 358:115005
24. Islam MS, Sultana J, Rifat AA, Ahmed R, Dinovitser A, Ng BWH, Heidepriem HE, Abbott D (2018) Dual-polarized highly sensitive plasmonic sensor in the visible to near-IR spectrum. Opt Express 26:30347–30361

Publisher's Note